

Induced magnetic form factor of chromium*

K. H. Oh, B. N. Harmon, S. H. Liu, and S. K. Sinha[†]

Ames Laboratory—Energy Research and Development Administration, Iowa State University, Ames, Iowa 50010

(Received 14 January 1976)

Expressions in terms of Bloch wave functions are derived for the induced nondiagonal magnetic susceptibility $\chi(\vec{G}, 0)$. The expressions for the important contributions are shown to reduce in the tight-binding limit to the usual Pauli spin, Van Vleck orbital, and core diamagnetic terms. Each of these contributions was evaluated for Cr using augmented-plane-wave energy bands and wave functions. The results are in good agreement with the recent measurement of the induced magnetic form factor by Stassis, Kline, and Sinha if an exchange enhancement factor of 2.53 is assumed for the spin contribution. The calculated orbital form factor is isotropic and is essentially identical to the free-ion orbital form factor of Freeman and Watson. The limitations and reasons for the success of the free-ion model are discussed.

I. INTRODUCTION

For metals the electronic response to an applied magnetic field has always been a fascinating but difficult problem. The basic complexities introduced by the electron-electron interactions are well known, and the separate orbital and spin contributions to the total magnetic response have been studied theoretically. It is not as easy to study these individual contributions experimentally, but by using the results of different experiments which give direct information about the microscopic response the various contributions may be separated. A classic example is the use of Knight-shift measurements to determine the contributions arising from the spin paramagnetism, the orbital paramagnetism, and the core diamagnetism.¹ Neutron diffraction is another extremely powerful microscopic probe which is used to study magnetic response. By analyzing the measured magnetic form factor it is possible to study the separate contributions to the net magnetic moment. This is because there is a different characteristic spatial distribution associated with each of the different response mechanisms. In this paper we are interested in obtaining further insight into the magnitude and character of the spatial response of Bloch electrons subject to a weak applied field. Using linear-response theory, expressions in terms of Bloch electrons are derived for the magnetic form factor which reduce to known results in the tight-binding and free-electron limits. The expressions for the larger contributions have the advantage of being physically transparent and are adaptable for accurate calculations, which is demonstrated by evaluating the induced magnetic form factor of Cr. The results are compared with the experimental form factor of Stassis, Kline, and Sinha,² which first motivated this work.

Moon, Koehler, and Trego have measured the neutron magnetic form factor of Cr in the ordered

state.³ Their measurements were made at the antiferromagnetic scattering angles and indicated that the ordered magnetization density could be fit well with an atomic $3d$ spin form factor. Later band calculations by Asano and Yamashita⁴ for the antiferromagnetic state of Cr also yielded a spin density which was in good agreement with the experiment. The more recently measured induced magnetic form factor² was found to be more extended than the form factor of Moon *et al.* and was also found to remain unchanged when the temperature was lowered through the Néel point. Gyromagnetic measurements suggest that the reason for the more extended induced magnetic form factor is the addition of an orbital contribution to the induced magnetization. In fact, using the $3d$ free-ion form factors of Freeman and Watson,⁵ Stassis *et al.* were able to fit their measured form factor using 60% orbital and 40% spin contributions. This predicts a gyromagnetic ratio of 1.25 compared to the experimental value of 1.21 ± 0.07 as measured by Einstein-de Haas experiments.⁶

The large orbital contribution to the induced magnetization in Cr is typical of transition metals which have nearly half-filled d bands, and arises from the Van Vleck paramagnetic susceptibility as first pointed out by Kubo and Obata.⁷ More recent band calculations of the Van Vleck paramagnetic susceptibility for Cr agree with the atomic-model results of Stassis *et al.* and yield a value of $\sim 100 \times 10^{-6}$ emu/mole for the orbital susceptibility.⁸ There is no reason to believe, however, that the spatial distribution of the induced orbital magnetization density will be well described by an atomic model since the solid-state wave functions can differ considerably from the corresponding atomic orbitals. The only way to tell why the atomic model for the form factor works as well as it does, and to assess its limitations, is to understand the details of the electron response in the metal. To this end we have used

linear-response theory to obtain expressions for the induced q -dependent magnetic susceptibility in the solid. We then selected the expressions corresponding to the dominant contributions to the magnetization and evaluated them using augmented-plane-wave (APW) wave functions. It should be noted that we have used a completely nonrelativistic approach which leaves out the effects of spin-orbit coupling. Although for Cr the spin-orbit coupling should be quite small, it could become important for heavier metals.

The linear-response formalism developed in Sec. II is similar to the treatment by Hebborn and March⁹ except that more emphasis is given to the tight-binding limit, which gives a fair description of the d electrons in Cr. We also concentrate on the nondiagonal q -dependent susceptibility, which is the one relevant to the neutron measurements. In addition to the Pauli spin paramagnetism and the Van Vleck orbital magnetism, the general expression for the susceptibility is also shown to contain the Landau-Peierls diamagnetic contribution, and the core diamagnetism. There is also a contribution arising from the itinerant nature of the conduction electrons which can be expressed in terms of surface integrals over the unit-cell boundary similar to the terms obtained by Yafet in considering the g value for conduction electrons.¹⁰ Because of the small value of the d wave functions at the cell boundary these surface terms are expected to be small and are not included in the total form-factor calculation. The details of the calculation for the spin and orbital form factors of Cr are given in Sec. III, and the final results and conclusions are given in Sec. IV.

II. FORMULATION

A. Linear-response theory for the generalized susceptibility

In this section we present the formulation of the orbital moment and the corresponding magnetic form factor induced by a uniform static magnetic field. The one-electron model of the metal is described by the Hamiltonian

$$H_0 = P^2/2m + V(\vec{r}), \quad (2.1)$$

where the potential satisfies the translation symmetry of the crystal,

$$V(\vec{r} + \vec{R}) = V(\vec{r}), \quad (2.2)$$

and \vec{R} is an arbitrary lattice vector of the crystal. For an infinite crystal the eigenstates of the Hamiltonian are the Bloch states

$$H_0 \psi_{n\vec{k}}(\vec{r}) = E_{n\vec{k}} \psi_{n\vec{k}}(\vec{r}), \quad (2.3)$$

where n is the band index and the wave vector \vec{k}

determines the phase shift of the Bloch wave function under translation,

$$\psi_{n\vec{k}}(\vec{r} + \vec{R}) = e^{i\vec{k} \cdot \vec{R}} \psi_{n\vec{k}}(\vec{r}), \quad (2.4)$$

and $E_{n\vec{k}}$ is the band energy. The wave functions are normalized in the unit cell.

The presence of a magnetic field modifies the Hamiltonian according to

$$H = \frac{1}{2m} \left(\vec{p} - \frac{e}{c} \vec{A}(\vec{r}) \right)^2 + V(\vec{r}), \quad (2.5)$$

where $\vec{A}(\vec{r})$ is the vector potential, which is related to the field by

$$\vec{B}(\vec{r}) = \nabla \times \vec{A}(\vec{r}). \quad (2.6)$$

For a static field with a sinusoidal spatial dependence $\vec{B}(\vec{r}) = \vec{B} e^{i\vec{q} \cdot \vec{r}}$, the vector potential may easily be solved in the transverse gauge, i.e., $\nabla \cdot \vec{A} = 0$.

The result is

$$\vec{A}(\vec{r}) = (i\vec{q} \times \vec{B}/q^2) e^{i\vec{q} \cdot \vec{r}}. \quad (2.7)$$

For magnetic fields generated in the laboratory the perturbation on the crystal is exceedingly small, so we will consider the vector potential as a perturbation and study the linear response of the system.

The magnetic moment density $M(\vec{r})$ induced by the field has a more complicated spatial dependence because of the nonuniform electron density in the metal. However, for two points in the metal separated by a lattice vector \vec{R} , the local magnetizations are in the same ratio as the local fields. This implies the following Bloch condition:

$$\vec{M}(\vec{r} + \vec{R}) = e^{i\vec{q} \cdot \vec{R}} \vec{M}(\vec{r}). \quad (2.8)$$

Hence, upon Fourier transformation

$$\vec{M}(\vec{r}) = \vec{M}(\vec{Q}) e^{i\vec{Q} \cdot \vec{r}}, \quad (2.9)$$

where the allowed \vec{Q} vectors are $\vec{Q} = \vec{G} + \vec{q}$, and \vec{G} is an arbitrary reciprocal-lattice vector. We can now define the generalized susceptibility $\chi_{ij}(\vec{Q}, \vec{q})$ by

$$M_i(\vec{Q}) = \lim_{\vec{q} \rightarrow 0} \sum_j \chi_{ij}(\vec{Q}, \vec{q}) B_j. \quad (2.10)$$

If B is along a high-symmetry direction of a cubic crystal, the induced moment is in the same direction. We call this the z direction; then the induced-moment form factor is proportional to

$$\chi_{zz}(\vec{G}, 0) = \lim_{\vec{q} \rightarrow 0} \chi_{zz}(\vec{G} + \vec{q}, \vec{q}), \quad (2.11)$$

and the bulk static susceptibility is

$$\chi = \lim_{\vec{q} \rightarrow 0} \chi_{zz}(\vec{q}, \vec{q}). \quad (2.12)$$

To apply the linear-response theory we need to

relate the magnetic moment density to the induced current through

$$\vec{J}(\vec{r}) = c \nabla \times \vec{M}(\vec{r}), \quad (2.13)$$

or, in terms of Fourier components,

$$\vec{J}(\vec{Q}) = ic \vec{Q} \times \vec{M}(\vec{Q}). \quad (2.14)$$

The magnetic field satisfies $\vec{q} \cdot \vec{B} = 0$. Since \vec{M} is parallel to \vec{B} , we have $\vec{Q} \cdot \vec{M}(\vec{Q}) = 0$ for all \vec{Q} 's parallel to \vec{q} . This allows us to solve for $\vec{M}(\vec{Q})$:

$$\vec{M}(\vec{Q}) = i \vec{Q} \times \vec{J}(\vec{Q}) / c Q^2. \quad (2.15)$$

Under these conditions the linear-response theory gives the following expression for the generalized susceptibility^{9, 11}:

$$\begin{aligned} \chi_{ij}(\vec{Q}, \vec{q}) &= \frac{e^2}{c^2 Q^2 q^2} \sum_{\alpha\alpha'} \frac{f_\alpha - f_{\alpha'}}{E_{\alpha'} - E_\alpha} \langle \alpha | [\vec{Q} \times \vec{J}(\vec{Q})]_i | \alpha' \rangle \\ &\quad \times \langle \alpha' | [\vec{q} \times \vec{J}^+(\vec{q})]_j | \alpha \rangle \\ &\quad - \frac{e^2}{m c^2 Q^2 q^2} (\vec{Q} \cdot \vec{q} \delta_{ij} - Q_i q_j) \\ &\quad \times \sum_{\alpha} f_{\alpha} \langle \alpha | e^{-i \vec{G} \cdot \vec{r}} | \alpha \rangle, \end{aligned} \quad (2.16)$$

where $|\alpha\rangle, |\alpha'\rangle$ are eigenstates of H_0 with eigenvalues $E_\alpha, E_{\alpha'}$; $f_\alpha, f_{\alpha'}$ are the Fermi distribution functions, and the current operator is

$$\vec{J}(\vec{Q}) = (1/2m) (\vec{p} e^{-i \vec{Q} \cdot \vec{r}} + e^{-i \vec{Q} \cdot \vec{r}} \vec{p}). \quad (2.17)$$

As mentioned previously the vectors \vec{q} , \vec{Q} , and \vec{G} are collinear. This does not restrict the generality of Eq. (2.17) because we always take the limit $\vec{q} \rightarrow 0$ in the end. So as long as \vec{G} is perpendicular to \vec{B} or \vec{M} , as in the actual experiments, we may choose \vec{q} parallel to \vec{G} and obtain the gen-

eralized susceptibility. With the static field in the z direction and the reciprocal-lattice vector \vec{G} normal to \vec{B} , say in the y direction, the generalized susceptibility expression reduces to

$$\begin{aligned} \chi_{zz}(Q, q) &= \frac{e^2}{c^2 Q q} \sum_{\alpha\alpha'} \frac{f_\alpha - f_{\alpha'}}{E_{\alpha'} - E_\alpha} \\ &\quad \times \langle \alpha | j_x(Q) | \alpha' \rangle \langle \alpha' | j_x(q) | \alpha \rangle \\ &\quad - \frac{e^2}{m c^2 Q q} \sum_{\alpha} f_{\alpha} \langle \alpha | e^{-i G y} | \alpha \rangle, \end{aligned} \quad (2.18)$$

with

$$j_x(Q) = (1/m) P_x e^{-i Q y},$$

and the bulk susceptibility reduces to

$$\chi_{zz}(q, q) = \frac{e^2}{c^2 q^2} \sum_{\alpha\alpha'} \frac{f_\alpha - f_{\alpha'}}{E_{\alpha'} - E_\alpha} |\langle \alpha | j_x(Q) | \alpha' \rangle|^2 - \frac{e^2 N}{m c^2 q^2}. \quad (2.19)$$

B. Uniform-field limit

In the uniform-field limit, $q \rightarrow 0$, both terms in the form factor, Eq. (2.18), diverge like q^{-1} , and those in the bulk susceptibility, Eq. (2.19), diverge like q^{-2} . This divergence arises because the vector potential for a uniform static field diverges in an infinite crystal. However, we will show in Appendix A that the diverging parts of the two terms exactly cancel for a finite crystal, so both the neutron form factor and the bulk susceptibility are finite. Then the surface of the crystal is no longer relevant and we may take the eigenstates $|\alpha\rangle$ to be the Bloch states $|n\vec{k}\rangle$ for the infinite crystal. After removing the divergent parts, we obtain for the neutron form factor

$$\chi_{zz}(G, 0) = \frac{2e^2 N}{m^2 c^2 G} \lim_{q \rightarrow 0} \frac{\partial}{\partial q} \left(\sum_{n'n\vec{k}} \frac{f_{n\vec{k}} - f_{n'\vec{k}+\vec{q}}}{E_{n',\vec{k}+\vec{q}} - E_{n\vec{k}}} \langle n\vec{k} | P_x e^{-i(G+q)y} | n', \vec{k} + \vec{q} \rangle \langle n', \vec{k} + \vec{q} | P_x e^{iqy} | n\vec{k} \rangle \right), \quad (2.20)$$

and the expression for the bulk susceptibility

$$\chi = \frac{2e^2 N}{m^2 c^2} \lim_{q \rightarrow 0} \frac{1}{2} \frac{\partial^2}{\partial q^2} \left(\sum_{n'n\vec{k}} \frac{f_{n\vec{k}} - f_{n'\vec{k}+\vec{q}}}{E_{n',\vec{k}+\vec{q}} - E_{n\vec{k}}} |\langle n\vec{k} | P_x e^{-iqy} | n', \vec{k} + \vec{q} \rangle|^2 \right). \quad (2.21)$$

The matrix elements are evaluated in the unit cell, N is the total number of atoms in the specimen, the sum on k is carried out in the first Brillouin zone, and the factor 2 accounts for the spin degeneracy. The evaluation of the derivatives is rather complicated. Before we exhibit the general results we will show that the formulas (2.20) and (2.21) reduce to all the known results in the extreme tight-binding limit and the free-electron limit.

In the extreme tight-binding limit the band en-

ergies are independent of \vec{k} and the wave functions are

$$\psi_{n\vec{k}}(\vec{r}) = \frac{1}{N^{1/2}} \sum_i e^{i\vec{k} \cdot \vec{R}_i} \psi_n(\vec{r} - \vec{R}_i), \quad (2.22)$$

where \vec{R}_i is the position of the i th atom, the sum on i is carried over the entire crystal, the atomic wave function $\psi_n(\vec{r} - \vec{R}_i)$ is centered at \vec{R}_i , and there is no overlap between the atomic wave functions centered at different sites. In this extreme

limit the intraband contributions are not considered. The bulk susceptibility can be found to be

$$\chi = \frac{2e^2 N}{m^2 c^2} \sum_{nn'} \frac{f_n - f_{n'}}{E_{n'} - E_n} (|\langle n | P_x y | n' \rangle|^2 - \langle n | P_x y^2 | n \rangle \langle n' | P_x | n \rangle), \quad (2.23)$$

where $|n\rangle$ is just $\psi_n(\vec{r})$ and the integrals are over a single cell. A few simple transformations with the help of the identities

$$\begin{aligned} [H_0, X_i] &= -i\hbar P_i/m, \\ [H_0, X_i X_j] &= -(i\hbar/m)(P_i X_j + X_j P_i) \end{aligned} \quad (2.24)$$

enable us to put the result in a more familiar form (see Appendix A):

$$\begin{aligned} \chi &= \frac{e^2 N}{2m^2 c^2} \sum_{nn'} \frac{f_n - f_{n'}}{E_{n'} - E_n} |\langle n | L_x | n' \rangle|^2 \\ &\quad - \frac{e^2 N}{m c^2} \sum_n f_n \langle n | x^2 + y^2 | n \rangle. \end{aligned} \quad (2.25)$$

The first term in the above expression is the Van Vleck susceptibility,¹² which is most important for transition-metal ions whose orbital moments are quenched by the crystal field. The appearance of the Fermi distribution function makes certain that the initial states are occupied and the intermediate states unoccupied. The second term is simply the core diamagnetic susceptibility.

The form factor may be similarly simplified. The result is

$$\begin{aligned} \chi_{xx}(G, 0) &= -\frac{ie^2 N}{m^2 c^2 G} \sum_{nn'} \frac{f_n - f_{n'}}{E_{n'} - E_n} \langle n | P_x e^{-iGy} | n' \rangle \\ &\quad \times \langle n' | L_x | n \rangle \\ &\quad - \frac{ie^2 N}{m c^2 G} \sum_n f_n \langle n | y e^{-iGy} | n \rangle. \end{aligned} \quad (2.26)$$

$$\begin{aligned} \chi_{xx}^{(1)}(G, 0) &= \frac{2e^2 N}{m^2 c^2 G} \sum_{nn', \vec{k}} \frac{f_{n\vec{k}} - f_{n'\vec{k}}}{E_{n'\vec{k}} - E_{n\vec{k}}} \\ &\quad \times \left(- \left\langle U_{n\vec{k}} \left| (P_x + \hbar k_x) e^{-iGy} \right| \frac{\partial U_{n'\vec{k}}}{\partial k_y} \right\rangle \langle n' \vec{k} | P_x | n \vec{k} \rangle + \langle n \vec{k} | P_x e^{-iGy} | n' \vec{k} \rangle \left\langle \frac{\partial U_{n'\vec{k}}}{\partial k_y} \left| P_x + \hbar k_x \right| U_{n\vec{k}} \right\rangle \right), \end{aligned} \quad (2.31)$$

which arises from differentiating the matrix elements, and

$$\chi_{xx}^{(2)}(G, 0) = \frac{2e^2 N}{m^2 c^2 G} \sum_{nn', \vec{k}} \left(\lim_{q \rightarrow 0} \frac{\partial}{\partial q} \frac{f_{n\vec{k}} - f_{n', \vec{k} + \vec{q}}}{E_{n', \vec{k} + \vec{q}} - E_{n\vec{k}}} \right) \langle n \vec{k} | P_x e^{-iGy} | n' \vec{k} \rangle \langle n' \vec{k} | P_x | n \vec{k} \rangle, \quad (2.32)$$

which arises from differentiating the band energies. In these equations the integrals for the matrix elements are again only over a single unit cell. In the extreme tight-binding limit $\chi_{xx}^{(1)}$ reduces to Eq. (2.26) and $\chi_{xx}^{(2)}$ vanishes. In the free-electron limit both terms vanish.

The term $\chi_{xx}^{(2)}$ may be put in a different form which avoids the limiting process of $q \rightarrow 0$. We divide the

The first term is the form factor associated with the Van Vleck paramagnetism and the second term is associated with the core diamagnetism. In the limit $G \rightarrow 0$ this expression reduces to the bulk susceptibility limit of Eq. (2.25) provided that there is complete symmetry between x and y , as in a cubic crystal with B in a high-symmetry direction. To arrive at this limit one must make use of the identities in Eq. (2.24) [also see Eq. (2.41)].

In the free-electron limit the wave functions and energies are

$$\psi_{\vec{k}} = \Omega^{-1/2} e^{-i\vec{k} \cdot \vec{r}}, \quad E_{\vec{k}} = \hbar^2 k^2 / 2m, \quad (2.27)$$

where Ω is the unit-cell volume. There is only one band, and the sum on \vec{k} is over the entire volume of \vec{k} space. It is easy to see that the form factor is identically zero for $G \neq 0$. The bulk susceptibility is

$$\begin{aligned} \chi &= \frac{2e^2 N \hbar^2}{m^2 c^2} \lim_{q \rightarrow 0} \frac{\partial^2}{\partial q^2} \sum_{\vec{k}} \frac{f_{\vec{k}} k_x^2}{E_{\vec{k} + \vec{q}} - E_{\vec{k}}} \\ &= -\frac{e^2 V k_F}{12 \pi^2 m c^2}, \end{aligned} \quad (2.28)$$

where $V = N\Omega$. This is just the Landau susceptibility.

For the general band problem we must differentiate all quantities that depend on q . The calculation is easier if we write

$$\psi_{n\vec{k}}(\vec{r}) = |n\vec{k}\rangle = e^{i\vec{k} \cdot \vec{r}} U_{n\vec{k}}(\vec{r}), \quad (2.29)$$

where $U_{n\vec{k}}(\vec{r})$ is the periodic part of the Bloch wave function. The form factor is found to have two kinds of terms:

$$\chi_{xx}(G, 0) = \chi_{xx}^{(1)}(G, 0) + \chi_{xx}^{(2)}(G, 0), \quad (2.30)$$

where

sum into intraband and interband terms. The interband terms can easily be differentiated. For the intraband terms we write

$$\frac{f_{n\vec{k}} - f_{n',\vec{k}+\vec{q}}}{E_{n',\vec{k}+\vec{q}} - E_{n\vec{k}}} = -\frac{\partial f_{n\vec{k}}}{\partial E_{n\vec{k}}} - \frac{1}{2}q \frac{\partial E_{n\vec{k}}}{\partial k_y} \frac{\partial^2 f_{n\vec{k}}}{\partial E_{n\vec{k}}^2} + O(q^2).$$

When this expression is substituted into the intraband terms the first term on the right-hand side gives no q dependence, hence no contribution. For the second term we transform the sum on \vec{k} into a surface integral over the constant-energy surface $E = E_{n\vec{k}}$ and an integral on E . Then a partial integration transforms the intraband term into the energy derivative of a constant-energy surface integral evaluated at the Fermi energy E_F . The final result is

$$\chi_{zz}^{(2)}(G, 0) = -\frac{2e^2 N}{m^2 c^2 G} \sum_{nn'} \left((1 - \delta_{nn'}) \sum_{\vec{k}} \frac{2f_{n\vec{k}}}{(E_{n',\vec{k}} - E_{n\vec{k}})^2} \frac{\partial E_{n',\vec{k}}}{\partial k_y} \langle n\vec{k} | P_x e^{-iGy} | n'\vec{k} \rangle \langle n'\vec{k} | P_x | n\vec{k} \rangle \right. \\ \left. + \frac{\Omega}{(2\pi)^3} \delta_{nn'} \frac{\partial}{\partial E_F} \oint_{E_F} \frac{dS}{|\nabla E_{n\vec{k}}|} \frac{\partial E_{n\vec{k}}}{\partial k_y} \langle n\vec{k} | P_x e^{-iGy} | n\vec{k} \rangle \langle n\vec{k} | P_x | n\vec{k} \rangle \right), \quad (2.33)$$

where $\nabla E_{n\vec{k}}$ is the \vec{k} gradient of $E_{n\vec{k}}$ and is normal to the constant-energy surface, and the symbol

$$\frac{\partial}{\partial E_F} \oint_{E_F} F(E_{n\vec{k}}) dS$$

for an arbitrary function $F(E_{n\vec{k}})$ of the energy means

$$\lim_{E \rightarrow E_F} \frac{\partial}{\partial E} \oint_{E_{n\vec{k}}=E} F(E_{n\vec{k}}) dS. \quad (2.34)$$

At this step we have completely removed the interim variable q from the formulation.

A similar series of manipulations may be carried out for the bulk susceptibility but, since there are two differentiations, we obtain three kinds of terms. These are

$$\chi^{(11)} = \frac{2e^2 N}{m^2 c^2} \sum_{nn'} \frac{f_{n\vec{k}} - f_{n'\vec{k}}}{E_{n',\vec{k}} - E_{n\vec{k}}} \left(\left| \langle U_{n\vec{k}} | P_x + \hbar k_x \left| \frac{\partial U_{n'\vec{k}}}{\partial k_y} \right. \right|^2 + \text{Re} \langle n'\vec{k} | P_x | n\vec{k} \rangle \langle U_{n\vec{k}} | P_x + \hbar k_x \left| \frac{\partial^2 U_{n'\vec{k}}}{\partial k_y^2} \right. \right), \quad (2.35)$$

$$\chi^{(22)} = \frac{e^2 N}{m^2 c^2} \sum_{nn'} \left\{ (1 - \delta_{nn'}) \sum_{\vec{k}} f_{n\vec{k}} \left(\frac{2(\partial E_{n',\vec{k}}/\partial k_y)^2}{(E_{n',\vec{k}} - E_{n\vec{k}})^3} - \frac{\partial^2 E_{n',\vec{k}}/\partial k_y^2}{(E_{n',\vec{k}} - E_{n\vec{k}})^2} \right) |\langle n'\vec{k} | P_x | n\vec{k} \rangle|^2 \right. \\ \left. - \frac{\Omega}{(2\pi)^3} \delta_{nn'} \left[\frac{1}{2} \frac{\partial}{\partial E_F} \oint_{E_F} \frac{dS}{|\nabla E_{n\vec{k}}|} \frac{\partial^2 E_{n\vec{k}}}{\partial k_y^2} |\langle n\vec{k} | P_x | n\vec{k} \rangle|^2 \right. \right. \\ \left. \left. - \frac{1}{3} \frac{\partial^2}{\partial E_F^2} \oint_{E_F} \frac{dS}{|\nabla E_{n\vec{k}}|} \left(\frac{\partial E_{n\vec{k}}}{\partial k_y} \right)^2 |\langle n\vec{k} | P_x | n\vec{k} \rangle|^2 \right] \right\}, \quad (2.36)$$

and

$$\chi^{(12)} = -\frac{2e^2 N}{m^2 c^2} \sum_{nn'} \left((1 - \delta_{nn'}) \sum_{\vec{k}} f_{n\vec{k}} \frac{2(\partial E_{n',\vec{k}}/\partial k_y)}{(E_{n',\vec{k}} - E_{n\vec{k}})^2} 2 \text{Re} \langle U_{n\vec{k}} | P_x + \hbar k_x \left| \frac{\partial U_{n'\vec{k}}}{\partial k_y} \right. \right) \langle n'\vec{k} | P_x | n\vec{k} \rangle \\ + \frac{\Omega}{(2\pi)^3} \delta_{nn'} \frac{1}{2} \frac{\partial}{\partial E_F} \oint_{E_F} \frac{dS}{|\nabla E_{n\vec{k}}|} \frac{\partial E_{n\vec{k}}}{\partial k_y} 2 \text{Re} \langle U_{n\vec{k}} | P_x + \hbar k_x \left| \frac{\partial U_{n'\vec{k}}}{\partial k_y} \right. \rangle \langle n'\vec{k} | P_x | n\vec{k} \rangle. \quad (2.37)$$

The term $\chi^{(11)}$ comes from differentiating the matrix elements twice with respect to q , $\chi^{(22)}$ from differentiating the band energies twice, and $\chi^{(12)}$ is the cross term between differentiating the matrix elements once and the energies once. In the tight binding limit $\chi^{(11)}$ reduces to the sum of the Van Vleck paramagnetic susceptibility and the core diamagnetic susceptibility, while $\chi^{(22)}$ and $\chi^{(12)}$ vanish because the band energies become independent of k , and in this limit there are no

intraband band contributions. In the free-electron limit $\chi^{(22)}$ reduces to the Landau diamagnetic susceptibility while $\chi^{(11)}$ and $\chi^{(12)}$ vanish.

C. Formulas used in computation

The formulas (2.32)–(2.37) for the form factor and the bulk susceptibility are still not practical for computational purposes. We will further manipulate the formulas in order to extract the

largest contribution in a calculable form. Experiments indicate that the largest contribution to both the bulk susceptibility and the form factor is the Van Vleck paramagnetic term, so this term must be carefully calculated. Thus, for the form factor we calculate the closest possible approximation to $\chi_{zz}^{(1)}(G, 0)$ and for the bulk susceptibility the closest approximation to $\chi^{(11)}$.

The k_y derivative of the wave function $U_{n\vec{k}}(\vec{r})$ satisfies

$$\frac{\partial U_{n\vec{k}}}{\partial k_y} = -iyU_{n\vec{k}} + \frac{i\hbar^2}{2m} \sum_{n' \neq n} \frac{S(nn', \vec{k})}{E_{n\vec{k}} - E_{n'\vec{k}}} U_{n'\vec{k}}, \quad (2.38)$$

where $S(nn', \vec{k})$ is a surface integral over the boundary of the unit cell $S(\vec{r})$:

$$S(nn', \vec{k}) = \int_{S(\vec{r})} d\vec{S} \cdot [(\nabla\psi_{n'\vec{k}}) y \psi_{n\vec{k}} - \psi_{n'\vec{k}} \nabla(y\psi_{n\vec{k}})]. \quad (2.39)$$

This relation was first used by Yafet¹⁰ for the orbital susceptibility of Bloch electrons. For chromium the Fermi level lies nearly halfway between the bonding and antibonding d states. So the matrix elements are mostly between a pair of bonding and antibonding d -state wave functions. Since the antibonding wave functions are small near the Wigner-Seitz cell boundary, the surface integrals $S(nn', \vec{k})$ over the cell boundary will be small. We will ignore them henceforth. Then the quantity in the large parentheses in Eq. (2.31) becomes

$$\langle n\vec{k} | P_x y e^{-iGy} | n'\vec{k} \rangle \langle n'\vec{k} | P_x | n\vec{k} \rangle + \langle n\vec{k} | P_x e^{-iGy} | n'\vec{k} \rangle \langle n'\vec{k} | P_x y | n\vec{k} \rangle. \quad (2.40)$$

We write

$$P_x y = -\frac{1}{2} L_z + \frac{1}{2} (P_x y + P_y x)$$

and use the commutation relation in Eq. (2.24) to obtain

$$\langle n'\vec{k} | P_x y | n\vec{k} \rangle = -\frac{1}{2} \langle n'\vec{k} | L_z | n\vec{k} \rangle + (im/2\hbar) \langle n'\vec{k} | [H_0, xy] | n\vec{k} \rangle. \quad (2.41)$$

The last term is transformed into

$$\frac{im}{2\hbar} (E_{n'\vec{k}} - E_{n\vec{k}}) \langle n'\vec{k} | xy | n\vec{k} \rangle + \frac{i\hbar}{4} \int_{S(\vec{r})} d\vec{S} \cdot [(\nabla\psi_{n'\vec{k}}) xy \psi_{n\vec{k}} - \psi_{n'\vec{k}} \nabla(xy\psi_{n\vec{k}})]. \quad (2.42)$$

The surface integral in the last equation is neglected for the same reason cited previously for $S(nn', \vec{k})$. Then, after some simple manipulations,

we obtain

$$\chi_{zz}^{(1)}(G, 0) \cong \chi_{\text{VV}}(G, 0) + \chi_D(G, 0),$$

where

$$\chi_{\text{VV}}(G, 0) = -\frac{ie^2 N}{m^2 c^2 G} \sum_{nn'\vec{k}} \frac{f_{n\vec{k}} - f_{n'\vec{k}}}{E_{n'\vec{k}} - E_{n\vec{k}}} \langle n\vec{k} | P_x e^{-iGy} | n'\vec{k} \rangle \times \langle n'\vec{k} | L_z | n\vec{k} \rangle, \quad (2.43)$$

and

$$\chi_D(G, 0) = -\frac{ie^2 N}{m c^2 G} \sum_{n\vec{k}} f_{n\vec{k}} \langle n\vec{k} | y e^{-iGy} | n\vec{k} \rangle. \quad (2.44)$$

The quantity $\chi_{\text{VV}}(G, 0)$ is the generalized Van Vleck form factor and $\chi_D(G, 0)$ is the generalized Stassis form factor.¹³ These resemble the two terms in the tight-binding form-factor formula, Eq. (2.26), but with the atomic wave functions replaced by crystal wave functions. The neglect of surface integrals is only justified when at least one of the wave functions in the matrix element is localized and has a small magnitude at the cell boundary. The wave functions of d states with energies above E_F in Cr are localized. The sum of the intermediate states in Eq. (2.43) is rapidly convergent because the L_z operator has large matrix elements between d -type band states only.

When the same approximations are carried out on the bulk susceptibility $\chi^{(11)}$, we obtain

$$\chi^{(11)} \cong \chi_{\text{VV}} + \chi_D, \quad (2.45)$$

with

$$\chi_{\text{VV}} = \frac{e^2 N}{2m^2 c^2} \sum_{nn'\vec{k}} \frac{f_{n\vec{k}} - f_{n'\vec{k}}}{E_{n'\vec{k}} - E_{n\vec{k}}} |\langle n\vec{k} | L_z | n'\vec{k} \rangle|^2 \quad (2.45a)$$

and

$$\chi_D = -\frac{e^2 N}{m c^2} \sum_{n\vec{k}} f_{n\vec{k}} \langle n\vec{k} | x^2 + y^2 | n\vec{k} \rangle. \quad (2.45b)$$

We will also make a few remarks on how the other terms may be calculated. The interband terms in $\chi_{zz}^{(2)}$, $\chi^{(22)}$, and $\chi^{(12)}$ are amenable to numerical calculations with the help of the relations

$$\frac{\partial E_{n\vec{k}}}{\partial k_y} = \frac{\hbar}{m} \langle n\vec{k} | P_y | n\vec{k} \rangle \quad (2.46)$$

and

$$\frac{\partial^2 E_{n\vec{k}}}{\partial k_y^2} = \frac{\hbar^2}{m} \left(1 + 2 \sum_{n' \neq n} \frac{|\langle n\vec{k} | P_y | n'\vec{k} \rangle|^2}{E_{n\vec{k}} - E_{n'\vec{k}}} \right). \quad (2.47)$$

However, the convergence property of the sums on the intermediate states requires careful study.

The intraband terms involve energy derivatives of surface integrals over constant-energy surfaces. Although an attempt on this kind of calculation has been made, the precision of the numerical method is still too crude to yield reliable answers.¹⁴

III. INDUCED MAGNETIC FORM FACTOR OF CHROMIUM

In the formulation of Sec. II expressions were given in Eqs. (2.43) and (2.44) for the largest contributions to the orbital magnetic form factor. In this section we use these formulas to evaluate the induced orbital form factor of chromium. The induced spin form factor is also evaluated in order to compare the total (spin plus orbital) theoretical form factor to the experimental result of Stassis *et al.*² First we present the results of an APW calculation for paramagnetic chromium, emphasizing those aspects of the band and wave-function properties which are important for the magnetic-form-factor investigations. The numerical methods used to evaluate the spin and orbital form factors are then described and the calculated values presented for the separate contributions.

A. Bands and wave functions

The energy eigenvalues and eigenfunctions were obtained for the first six bands of Cr using the linearized version of the APW method.¹⁵ The crystal potential for this calculation was obtained by superposition of the Hartree-Fock-Slater $3d^5 4s^1$ atomic charge densities using the full value of the Slater exchange parameter ($\alpha=1$). Because wave functions have been found sensitive to non-muffin-tin corrections of the potential,¹⁶ a so-called warped-muffin-tin potential¹⁷ was used in which the actual potential between the spheres was taken into account. For a particular \vec{k} point the basis set was chosen to include all those reciprocal-lattice vectors \vec{K}_i such that

$$|\vec{k} + \vec{K}_i| R_{MT} \leq 7.0, \quad (3.1)$$

where R_{MT} is the muffin-tin sphere radius. This results in typically 45–55 basis functions and better than 2-mRy convergence on the energy eigenvalue.¹⁸

The bands and wave functions were obtained on a slightly compressed $\pi/6a$ mesh (140 points) in the irreducible $\frac{1}{48}$ th of the Brillouin zone. The compressed mesh moves the k points to be evaluated very slightly away from the high-symmetry points—just enough to break any degeneracies. It was found that this facilitates the interpolation of matrix elements and improves the Fourier-series fit of the bands which was obtained. The bands along the high-symmetry directions are shown in Fig. 1. Both the band structure and Fermi surface are in good agreement with previous work.¹⁹ In order to graphically present information about the l character of the various bands the l components of the calculated wave functions have been projected out and the k dependence least-squares fit with symmetrized plane waves. The fits are used to give a global representation of the l character throughout the Brillouin zone; however they are not able to reproduce the discontinuities which occur at band crossings. For this reason the l -dependence plots shown in Fig. 2 are smoother looking than is the actual case. These plots, however, do provide an excellent qualitative description of the wave-function character, and show how their l dependence changes in regions of hybridization. An l decomposition such as Fig. 2 is useful for understanding how certain matrix elements vary as function of k (e.g., optical matrix elements are expected to be large between a band pair in which one band has largely $l=1$ character and the other band $l=2$ character).

From Fig. 2 it is evident that bands 3 and 4, which are cut by the Fermi level, are mostly of

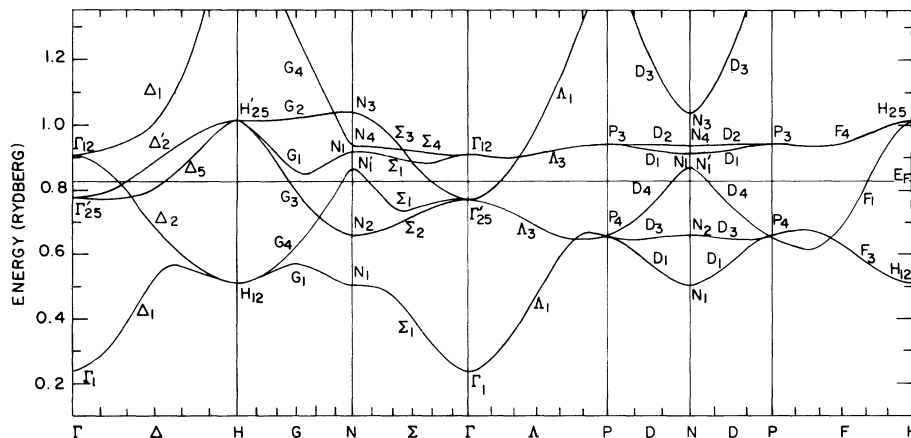


FIG. 1. Energy bands of Cr along the high-symmetry directions.

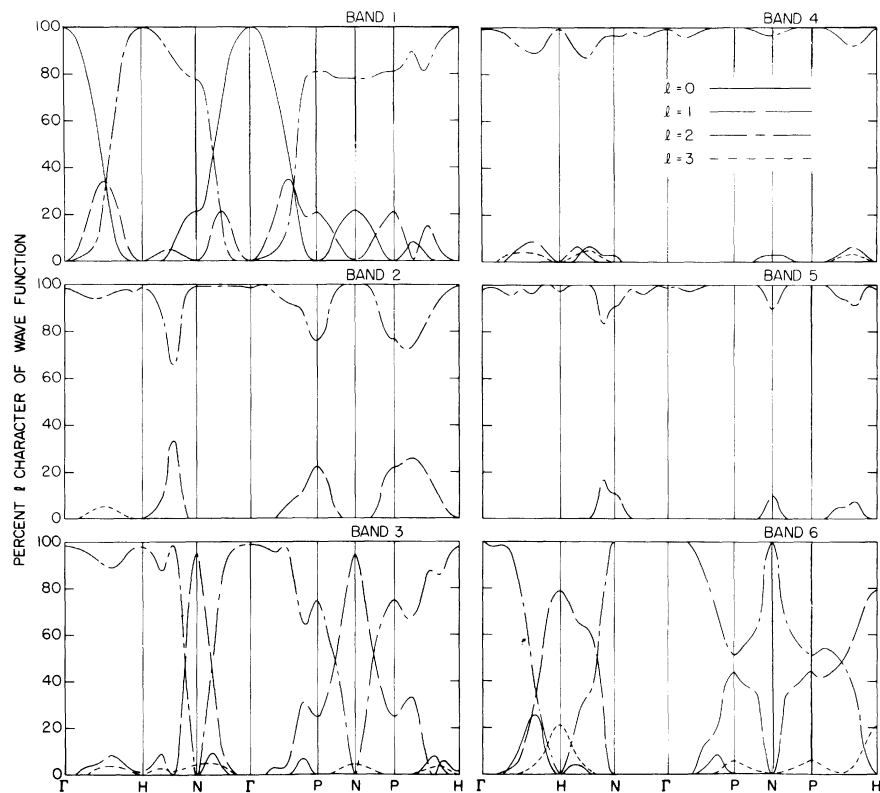


FIG. 2. Percentage of l character of Cr wave functions along the high-symmetry directions.

$l=2$ character except near the point N for band 3, where there is a predominance of $l=1$ character. The $l=2$ character of the wave functions on the Fermi surface gives rise to the d -like Pauli paramagnetic spin density. The $l=4$ character is not shown on these graphs, but did contribute as much as 3% in certain regions of the Brillouin zone. The $l=3$ character is fairly small, but does rise to about 20% of the band 6 wave function at the H point. In connection with these l -character decompositions it is natural to ask how reliable are the APW wave functions. A large degree of confidence was obtained by comparing the APW wave functions with Korringa-Kohn-Rostoker (KKR) wave functions for the Chodorow muffin-tin potential of copper. The KKR wave functions were expanded through $l=4$ and gave the same (three significant figures) l decomposition as was obtained by the APW method.²⁰ It should also be noted that for those wave functions with significant $l=3$ character (5% or greater) the energy eigenvalues, obtained by the KKR method with only up to $l=2$ radial decomposition, were poorly converged (10 mRy or greater).

The density of states of Cr is typical of the bcc transition metals and shows that the Fermi energy lies approximately in the middle of the d bands. The large Van Vleck orbital magnetic moment is a consequence of there being a large number of both

occupied and unoccupied d states. The occupied d states being lower in energy are more spread out (bonding character) than the antibonding unoccupied d states near the top of the d bands. This is demonstrated in Fig. 3, where the pure $l=2$ radial probability densities are shown for energies at the bottom, middle, and top of the d bands. In Fig. 3 the radial function obtained at $E=E_F=0.829$ Ry is just slightly more spread out than the Hartree-Fock-Slater $3d$ atomic function which was used to

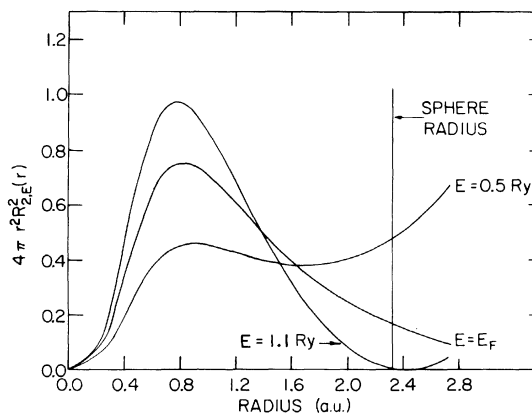


FIG. 3. Chromium $l=2$ radial probability densities for energies near the bottom, middle, and top of the d bands.

create the crystal potential. This leads to a slightly more contracted solid-state spin form factor compared with the atomic $3d$ form factor.

B. Induced spin form factor

If in Eq. (2.16) we substitute for $\vec{j}(\vec{Q})$ the spin current instead of the orbital current we obtain an

$$\chi_{zz}^{\text{spin}}(G, 0) = \lim_{\vec{q} \rightarrow 0} 2 \left(\frac{\hbar e}{2 m c} \right)^2 \sum_{\vec{k}, \vec{k}'} \frac{f_{n, \vec{k}} - f_{n', \vec{k} + \vec{q}}}{E_{n', \vec{k} + \vec{q}} - E_{n, \vec{k}}} \langle n, \vec{k} | e^{-i(G+\vec{q})y} | n', \vec{k} + \vec{q} \rangle \langle n', \vec{k} + \vec{q} | e^{i\vec{q}y} | n, \vec{k} \rangle, \quad (3.3)$$

where we have again taken the field along the z axis and \vec{Q} along the y direction, and have included the factor of 2 for the band spin degeneracy. Taking the limit of \vec{q} going to zero the spin susceptibility may be written

$$\chi_{zz}^{\text{spin}}(\vec{G}, 0) = \int \rho(\vec{r}) e^{-i\vec{G} \cdot \vec{r}} d^3r, \quad (3.4)$$

where

$$\rho(\vec{r}) = 2 \mu_B^2 \sum_n \oint_{E=E_F} \frac{dS(\vec{k})}{|\nabla_{\vec{k}} E(\vec{k})|} |\psi_{\vec{k}, n}(\vec{r})|^2 \quad (3.5)$$

is the spin density due to the conduction electrons at the Fermi surface. Note that since the wave functions are normalized, $\chi^{\text{spin}}(0, 0)$ is just the unenhanced Pauli susceptibility $2 \mu_B^2 D(E_F)$, where $D(E_F)$ is the density of states per spin at the Fermi energy.

Before presenting the calculated results, a general outline of the numerical procedures is in order to help the reader in better understanding the precision of the values obtained. All the k -space integrations in this paper were performed using the tetrahedron method^{21, 22} or some variation of it. In this method of Brillouin zone is divided into a large number of tetrahedrons. Within each tetrahedron the energy bands are obtained by linear interpolation between the energy eigenvalues evaluated at the four corners. In actual practice the number of tetrahedrons must be quite large if linear interpolation is to provide an accurate representation to the energy bands. In order to economically test the integral convergence with increasing the number of tetrahedrons, we obtained a global representation for each band by least-squares fitting the 140 APW band energies with 60 symmetrized plane waves. The rms error was the largest for band 5, being 2.6 mRy. From the fits the energies were generated on a π/Na mesh, and each π/Na cube was divided into six tetrahedrons. Convergence was tested up to $\pi/15a$; however, the $\pi/6a$ results were accurate to better than 2% for all the integrations. The $\pi/6a$ mesh was used the most, since the matrix elements were

expression for the induced spin susceptibility. The spin current is simply

$$\vec{j}(\vec{Q}) = (i\hbar/2m) \vec{Q} \times \vec{\sigma} e^{-i\vec{Q} \cdot \vec{r}} \quad (3.2)$$

and the resulting spin susceptibility

evaluated on this mesh and were more easily interpolated.

For the spin form factor, the integration in Eq. (3.5) was performed by using a $\pi/8a$ mesh of tetrahedrons. The energy gradient and the cross-sectional area for $E = E_F$ (a plane inside each tetrahedron) was found for each of the 202 inequivalent tetrahedrons containing the Fermi surface. The center of mass \vec{k}_i was evaluated for each Fermi-surface plane, and the wave functions for these wave vectors calculated. Each of the 202 charge densities $|\psi_{\vec{k}_i, n}(\vec{r})|^2$ were summed with the corresponding $\Delta S_i / |\nabla E(k_i)|$ weights to yield the induced spin density. The Fourier transform of Eq. (3.4) was taken and the unenhanced Pauli induced spin form factor obtained. The numerical results are listed in Table I and the normalized spin form factor is plotted in Fig 4. For the sake of comparison, Freeman and Watson's $3d$ free-ion spin form factor⁵ is also shown in this figure and indicates that the induced solid-state form factor is more contracted. In other words, the crystal charge density from states on the Fermi surface is slightly more extended than the $3d$ free-ion

TABLE I. Calculated values of the induced Pauli-type spin (χ_{spin}) and the Van Vleck-type orbital (χ_{VV}) form factors of Cr. The normalized values of χ_{spin} and χ_{VV} are shown in parentheses.

\vec{G}	$\sin\theta/\lambda$	χ_{spin} (10^{-6} emu/mole)	χ_{VV} (10^{-6} emu/mole)
[000]	0.000	18.79 (1.000)	130.00 (1.000)
[110]	0.245	7.52 (0.400)	87.36 (0.672)
[200]	0.347	3.68 (0.196)	60.32 (0.464)
[211]	0.425	2.84 (0.151)	...
[220]	0.490	1.88 (0.100)	...
[310]	0.548	0.66 (0.035)	...
[222]	0.600	1.20 (0.064)	...
[321]	0.649	0.56 (0.030)	...
[400]	0.693	-0.53 (-0.028)	16.43 (0.126)
[330]	0.735	0.23 (0.012)	14.12 (0.109)
[411]	0.735	-0.28 (-0.015)	...
[420]	0.775	-0.15 (-0.008)	...

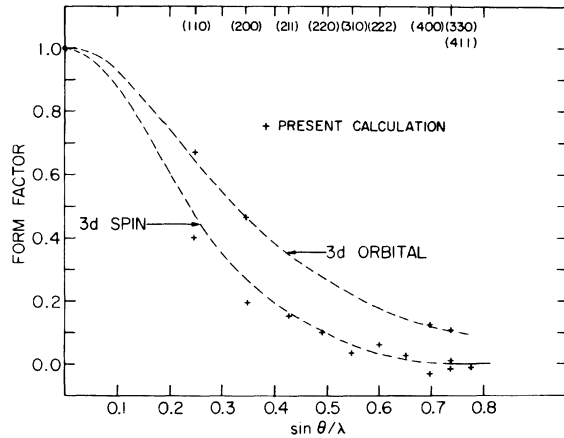


FIG. 4. Normalized spin and orbital magnetic form factors of Cr. The dashed curves are the form factors calculated from the $3d$ free-ion orbitals by Freeman and Watson (Ref. 5).

charge density.

The electron-electron interaction will further populate the spin-up states, resulting in an exchange-enhanced susceptibility. Similar to Pd,²³ the effect of exchange enhancement on the shape of the spin density (or the normalized form factor) is expected to be small. This is because the spatial distribution of the additional repopulated states is essentially the same as those spin-up states already included at the Fermi level. The strength of the exchange interaction is strongest for localized states, and since the electrons at the Fermi level in Cr are predominantly $l=2$ in character and have the same degree of localization, all regions of the Fermi surface will have about the same enhanced contribution. There is, however, some $l=1$ character on the Fermi surface near the point N of band 3, but the weight ($\Delta S|\nabla E|$) is small for this region. Just to be cautious, we re-summed the 202 tetrahedrons for Eq. (3.5) with an additional weighting on the $l=2$ states, to see if an increased proportion of localized states would alter our calculated spin form factor. Our results indicated no appreciable difference, so in the rest of this paper the normalized exchange-enhanced spin form factor is assumed to be the same as the unenhanced spin form factor shown in Fig. 4. We also neglect contributions due to core polarization, which is expected to be small.

C. Generalized Van Vleck orbital form factor

The induced Van Vleck paramagnetism arises from the applied field mixing higher excited states into the unperturbed ground state. Angular momentum for the new ground-state wave functions is not quenched and the expectation value of the

current operator yields the spatial distribution of the corresponding induced magnetization. This is the essence of Eq. (2.43),

$$\chi_{\mathbf{v}\mathbf{v}'}(G, 0) = -\frac{ie^2}{m^2c^2G} \sum_{nn'\mathbf{k}} \frac{f_{n\mathbf{k}} - f_{n'\mathbf{k}}}{E_{n'\mathbf{k}} - E_{n\mathbf{k}}} \langle n\mathbf{k} | P_x e^{-iGy} | n'\mathbf{k} \rangle \times \langle n'\mathbf{k} | L_x | n\mathbf{k} \rangle. \quad (2.43)$$

To evaluate this expression only bands 1–6 were included in the sum, since the d bands, which make the overwhelming contribution, are completely contained within this complex of bands.

The matrix elements needed were obtained on the $\pi/6a$ mesh for the required band pair. Only terms through $l=4$ were retained in the wave-function expansion inside each muffin-tin sphere, since the higher- l components were found to contribute less than 0.5%. The current matrix elements were precisely calculated using the formulas given in Appendix B; however, an approximation was made to facilitate the calculation of the angular momentum matrix elements. The APW radial functions were extended to the Wigner-Seitz sphere and the integrals evaluated within the sphere. This is a good approximation if the wave functions have small magnitude at the cell boundary, as is expected for the important d -like wave functions. An idea as to the accuracy of these matrix elements may be obtained by comparing the charge obtained within the Wigner-Seitz sphere with the correctly normalized value of 1.0. The Wigner-Seitz charge inside the sphere was calculated for each wave function and the s - p -like states were found to have the larger error (the greatest error was 10% with the average error less than 6%), while the more important d -like states were better behaved (the greatest error was 5% with the average error less than 2%). Each wave function was renormalized so that its Wigner-Seitz-sphere charge equaled 1.0. With this renormalization, we believe the angular momentum matrix elements are quite accurate.

For a cubic crystal the star of k has three independent angular momentum matrix elements, and the current operator has six and 12 independent matrix elements for $\vec{G}=(G_x, 0, 0)$ and $\vec{G}=(G_x, G_y, 0)$, respectively. The wave functions for the matrix elements which were needed outside the irreducible $\frac{1}{48}$ th of the Brillouin zone were obtained from those already calculated by group theory.

The k -space integration in Eq. (2.43) was performed by dividing each π/Na cube into six tetrahedrons and assuming linear energy dependence within each tetrahedron. In this way the energy denominator can be obtained analytically.^{24, 25} The matrix elements were assumed to be constant within each tetrahedron with their value obtained by

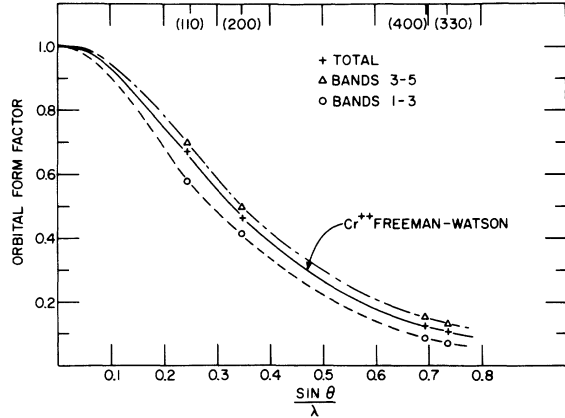


FIG. 5. Orbital form factor for band pairs 1-3 and 3-5 along with the total orbital form factor. The solid curve is the free-ion orbital form factor of Freeman and Watson (Ref. 5), while the dashed curves are drawn only as an aid to the eye.

local interpolation from the matrix elements tabulated on the $\pi/6a$ mesh. Using local interpolation the matrix element for the point \vec{k} (taken as the center of mass of the tetrahedron) is given by

$$M(\vec{k}) = \left(\sum_{i=1}^8 \frac{1}{|\vec{k} - \vec{k}_i|^L} M(\vec{k}_i) \right) / \left(\sum_{i=1}^8 \frac{1}{|\vec{k} - \vec{k}_i|^L} \right),$$

where the i sum is over the eight corners of the $\pi/6a$ cube which contains the \vec{k} point. L was varied between 1 and 7 to test the sensitivity to the interpolation. For $L=1$ the interpolation is nearly linear, and for $L=7$ the nearest $\pi/6a$ mesh point dominates. The results were very insensitive to L variations (less than 1% changes), so we report only those results obtained for $L=3$. The number of tetrahedrons was also varied by choosing different π/Na meshes. The results for $N \geq 6$ were all within a percent of each other.

The contributions from each of the allowed 13 band pairs were summed to give the Van Vleck orbital form factor listed in Table I. Only five values were obtained because of the large computational effort required. The bulk ($G=0$) Van Vleck susceptibility was calculated to be 130×10^{-6} emu/mole. The results are normalized to this value and shown in Fig. 4. The curve which passes through these points is the Freeman-Watson free ion 3d form factor. It is at first quite surprising that the solid-state form factor has the same shape as the free-ion form factor. It is surprising because in the ion the 3d orbitals have the same radial dependence and the angular momentum is a

ground-state property, whereas in the solid the angular momentum is quenched in the ground state and the angular momentum matrix elements are taken between occupied and unoccupied states with considerably different radial dependence (see Fig. 3). We believe this result is somewhat of a coincidence and arises because the Cr Fermi level falls in the middle of the d bands. There is thus an averaging effect between the spread out occupied wave functions in the lower bands and the more spatially contracted unoccupied wave functions in the higher bands. This effect is demonstrated in Fig. 5, where the normalized contributions from band pairs 1-3 and 3-5 are shown along with the total. The form factor for bands 1-3 is more contracted relative to the total because it involves the lower band 1, which has more spatially spread out wave functions, whereas the band-5 wave functions are more contracted because of their antibonding character and hence the 3-5 "transitions" yield a more expanded form factor.

Another feature apparent in Fig. 4 is the lack of any orbital anisotropy. The form factor was evaluated for $\vec{G}=(4, 0, 0)$ and $(3, 3, 0)$ because the anisotropy in the measured form factor was large for these reflections. However, within the accuracy of our calculation there is no orbital anisotropy. This does not contradict the experimental results since the anisotropy of the calculated spin form factor discussed in Sec. III B accounts for the measured anisotropy. Since the anisotropy is a purely solid-state effect, more precise experimental measurements would be useful in determining if there is any anisotropy from the orbital contribution to the magnetization density.

D. Diamagnetic form factor

The expression for the diamagnetic form factor is given in Eq. (2.44). In the tight-binding or atomic limit this contribution to the bulk susceptibility corresponds to the usual core diamagnetic susceptibility of Eq. (2.45b). For the core electrons it is convenient to write Eq. (2.44) as

$$\chi_D(G, 0) = \frac{e^2}{m c^2 G} \frac{\partial}{\partial G} \sum_{n\vec{k}} f_{n\vec{k}} \langle n\vec{k} | e^{-iGy} | n\vec{k} \rangle$$

and treat G as a continuous variable (see Ref. 13). The summation is just the charge-density form factor, which may be easily calculated and the numerical derivative taken. For the conduction electrons we again use the Wigner-Seitz approximation and rewrite Eq. (2.44) as

$$\chi_D(G, 0) = - \frac{4\pi e^2}{m c^2 G} \sum_{LM, lm} i^l Y_{lm}(\hat{G}) \int \left(\frac{i\sqrt{2}m}{3} (Y_{11} + Y_{1-1}) \right) Z_{LM}(\hat{r}) Y_{lm}^*(r) d\Omega \int_0^{R_{ws}} C_{LM}(r) j_l(Gr)^3 r^3 dr,$$

TABLE II. Calculated Stassis diamagnetic form factors for the core and the conduction electrons. The units are 10^{-6} emu/mole.

\vec{G}	Core ($1S^22S^22p^63S^23p^6$)	Conduction electron	Total
[000]	-14.417	-29.274	-43.691
[110]	-9.468	-5.050	-14.518
[200]	-6.467	-0.991	-7.458
[220]	-3.312	-0.314	-3.626
[310]	-2.470	-0.588	-3.058
[400]	-1.198	-0.134	-1.332
[330]	-0.991	-0.015	-0.976
[420]	-0.841	-0.057	-0.784
[510]	-0.586	-0.034	-0.620
[440]	-0.110	-0.046	0.064

where the charge density has been expanded in cubic harmonics $Z_{LM}(\hat{r})$:

$$\begin{aligned} \rho(\vec{r}) &= \sum_{n, \vec{k}} f_{n, \vec{k}} |\psi_{n, \vec{k}}(\vec{r})|^2 \\ &= \sum_{LM} C_{LM}(r) Z_{LM}(\hat{r}). \end{aligned}$$

The results of these calculations are presented in Table II. The conduction electrons contribute very little beyond the first reflection but give a very large contribution in the forward direction. It is interesting to note that the bulk diamagnetic susceptibility calculated from our atomic charge density was -59.124×10^{-6} emu/mole, which is 26% larger than the solid-state result. However, our solid-state result is for those currents restricted to within the Wigner-Seitz unit cell, and contributions from intercellular currents (e.g., the Landau diamagnetic contribution) may be important.

IV. RESULTS AND CONCLUSIONS

The total theoretical form factor is obtained by adding the Van Vleck orbital, the Pauli spin, and the diamagnetic form factors. Figure 6 shows this form factor compared with the experimental results of Stassis *et al.*² The spin form factor has been multiplied by an exchange enhancement factor of 2.53 (determined by least-squares fitting the total form factor at the four values of $\sin\theta/\lambda$). The agreement between theory and the neutron measurements is excellent; however, there is poor agreement between theory (at $\sin\theta/\lambda = 0$) and the measured bulk susceptibility. Given the exceptional agreement for finite scattering angles, this discrepancy for the bulk susceptibility is very intriguing. Most of the difference arises when the diamagnetic form factor is considered. It should

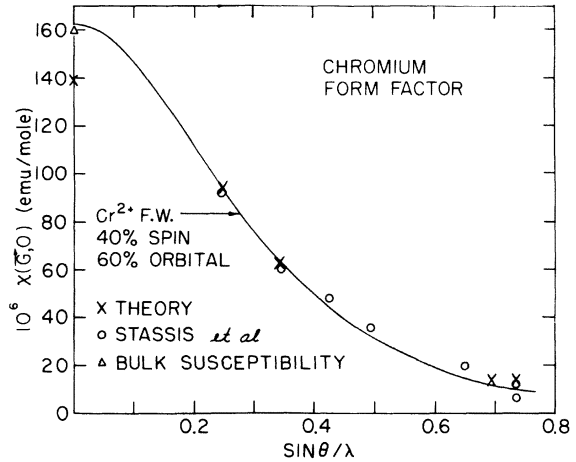


FIG. 6. Experimental neutron magnetic form factor of Stassis *et al.* (Ref. 2) and the total theoretical form factor. The solid curve is the free-ion result using a 40% spin and a 60% orbital contribution, but with no diamagnetic contribution.

be recalled that the atomic diamagnetic form factor is 26% larger at $G=0$ than the solid-state diamagnetic form factor, and would result in an even larger discrepancy. Since there most certainly is a diamagnetic contribution on the order we have calculated, the explanation for the higher measured value must be the neglect of additional paramagnetic contributions. These additional contributions must correspond to magnetization densities having relatively uniform spatial distributions in order to substantially increase only the $G=0$ "reflection." It is reasonable to expect such contributions are contained in the expressions we have not evaluated. In Sec. IIC we were concerned with obtaining formulas which were correct in the tight-binding limit, and neglected surface integrals over the unit cell because of the small value of the wave functions on this surface. These surface terms are nonzero for itinerant electrons, and presumably correspond to intercellular currents which would contribute at $G=0$. Thus the evaluation of these terms would be very interesting, although it is beyond the aim of the present paper in which we are primarily concerned with the orbital form factor.

The calculations for the orbital form factor indicate that the atomic model must be used with caution if the Fermi energy does not lie in the middle of the d -band complex. Of course, when the Fermi energy does lie in the middle of the d bands the Van Vleck paramagnetism is largest and thus the atomic model should be reasonable for the solids which have the largest Van Vleck contributions. In this respect it would be very interesting to perform accurate neutron diffraction

measurements on metals in which the Fermi energy is near the top or the bottom of the d bands and in which the gyromagnetic ratio is small enough to indicate a substantial orbital contribution (e.g., Ti). The calculated orbital form factor is isotropic. This may not be a general feature of orbital form factors for other metals which have less than cubic symmetry or higher atomic number so that spin-orbit coupling becomes important. Accurate measurements of the induced form-factor anisotropy for heavy metals with large orbital contributions coupled with the corresponding relativistic band and susceptibility calculations will shed light on this question.

ACKNOWLEDGMENT

We would like to express our gratitude to Dr. C. Stassis for many useful discussions.

APPENDIX A

We prove here that the two divergent terms in $\chi_{zz}(G+q, q)$ exactly cancel in the limit $q \rightarrow 0$. We single out from Eq. (2.18) the coefficients of q^{-1} from both terms. These are

$$T_1 = \frac{e^2}{m^2 c^2 G} \sum_{\alpha\alpha'} \frac{f_\alpha - f_{\alpha'}}{E_{\alpha'} - E_\alpha} \langle \alpha | P_x e^{-iGy} | \alpha' \rangle \langle \alpha' | P_x | \alpha \rangle,$$

$$T_2 = -\frac{e^2}{m c^2 G} \sum_{\alpha} f_\alpha \langle \alpha | e^{-iGy} | \alpha' \rangle.$$

Since

$$\langle \alpha' | P_x | \alpha \rangle = (im/\hbar) \langle \alpha' | H_0 x - x H_0 | \alpha \rangle,$$

$$\langle n\vec{k} | e^{-iGy} \nabla_y | n'\vec{k}' \rangle = \sum_{nn'} A_n^* A_{n'} i(\vec{k} + \vec{K}_n)_y \Omega \delta(\vec{G} + \vec{K}_n, -\vec{K}_n) - 4\pi r_{\text{MT}}^2 \frac{j_1(|\vec{G} + \vec{K}_n - \vec{K}_n| r_{\text{MT}})}{|\vec{G} + \vec{K}_n - \vec{K}_n|}, \quad (\text{B1})$$

where Ω is the unit-cell volume, \vec{K}_n 's are the reciprocal-lattice vectors associated with the plane waves, and the A_n are the corresponding APW expansion coefficients.

Second, with the angular decomposition of the wave functions inside the muffin-tin spheres, we seek matrix elements of $e^{i\vec{G} \cdot \vec{r}} \nabla_p$, where

$$\nabla_{\pm 1} = \mp \frac{1}{\sqrt{2}} \left(\frac{\partial}{\partial x} \pm i \frac{\partial}{\partial z} \right) \quad \text{and} \quad \nabla_0 = \frac{\partial}{\partial z}. \quad (\text{B2})$$

This becomes then

$$\langle n\vec{k} | e^{i\vec{G} \cdot \vec{r}} \nabla_p | n'\vec{k}' \rangle = \sum_{lm, l'm'} A_{lm}^* A_{l'm'} \langle lm | e^{i\vec{G} \cdot \vec{r}} \nabla_p | l'm' \rangle, \quad (\text{B3})$$

where the A_{lm} are the expansion coefficients for the wave functions inside the APW sphere. The last matrix element can be further reduced,

$$\langle lm | e^{i\vec{G} \cdot \vec{r}} \nabla_p | l'm' \rangle = 4\pi \sum_{k\theta} i^k Y_{k\theta}^*(\hat{G}) \int d\hat{r} Y_{lm}(\hat{r}) Y_{k\theta}(\hat{r}) \int dr r^2 j_k(Gr) R_l(r) [\nabla_p R_{l'}(r) Y_{l'm'}(\hat{r})], \quad (\text{B4})$$

where we have used the plane-wave expansion

and the Hamiltonian H is Hermitian for a finite crystal whose wave functions vanish rapidly outside the volume of the crystal, one obtains

$$\langle \alpha' | P_x | \alpha \rangle = (im/\hbar)(E_{\alpha'} - E_\alpha) \langle \alpha' | x | \alpha \rangle.$$

Then,

$$\begin{aligned} T_1 &= \frac{ie^2}{m c^2 G \hbar} \sum_{\alpha\alpha'} (f_\alpha - f_{\alpha'}) \langle \alpha | P_x e^{-iGy} | \alpha' \rangle \langle \alpha' | x | \alpha \rangle \\ &= \frac{ie^2}{m c^2 G \hbar} \sum_{\alpha} f_\alpha \langle \alpha | [P_x e^{-iGy}, x] | \alpha \rangle \\ &= -T_2. \end{aligned}$$

This completes the proof.

In a similar manner one can show that the q^{-2} terms in the bulk susceptibility exactly cancel. There is no q^{-1} term here because of the symmetry property

$$\chi_{zz}(q, q) = \chi_{zz}(-q, -q).$$

Thus the bulk susceptibility is also well behaved in the uniform-field limit.

The same manipulations are also used to transform the tight-binding result Eq. (2.23) into the more familiar form Eq. (2.25).

APPENDIX B

In this appendix, we show the expressions for the current matrix elements in terms of the APW wave functions. First, with the plane waves outside the muffin-tin spheres, it is easy to show that the current matrix elements become

$$e^{i\vec{G}\cdot\vec{r}} = 4\pi \sum_{k\theta} i^k j_k(Gr) Y_{k\theta}^*(\hat{G}) Y_{k\theta}(\hat{r}) \quad (\text{B5})$$

to obtain Eq. (B4) from Eq. (B3). Now we use the relation

$$\begin{aligned} \nabla_p [R_l(r) Y_{lm}(\hat{r})] &= (-1)^{l+1} (l+1)^{1/2} \left(\frac{d}{dr} - \frac{l}{r} \right) R_l(r) \sum_M \begin{pmatrix} 1 & l & l+1 \\ p & m & M \end{pmatrix} Y_{l+1, M}^*(\hat{r}) \\ &+ (-1)^l l^{1/2} \left(\frac{d}{dr} - \frac{l}{r} \right) R_l(r) \sum_M \begin{pmatrix} 1 & l & l-1 \\ p & m & M \end{pmatrix} Y_{l-1, M}^*(\hat{r}). \end{aligned} \quad (\text{B6})$$

Then, after the substitution of Eq. (B6), Eq. (B4) becomes

$$\begin{aligned} \langle lm | e^{i\vec{G}\cdot\vec{r}} \nabla_p | l'm' \rangle &= 4\pi \sum_{k\theta} i^k Y_{k\theta}^*(\hat{G}) (-1)^{p+m'+l'} \sum_{\theta_1} \left[(l'+1)^{1/2} G_{k\theta, l'+1, \theta_1}^{lm} \begin{pmatrix} l'+1 & 1 & l' \\ \theta_1 & -p & -m' \end{pmatrix} \right. \\ &\times \int dr r^2 j_k(Gr) R_l(r) \left(\frac{d}{dr} - \frac{l'}{r} \right) R_{l'}(r) + (l')^{1/2} G_{k\theta, l'-1, \theta_1}^{lm} \\ &\left. \times \begin{pmatrix} l'-1 & 1 & l' \\ \theta_1 & -p & -m' \end{pmatrix} \int dr r^2 j_k(Gr) R_l(r) \left(\frac{d}{dr} + \frac{l'+1}{r} \right) R_{l'}(r) \right]. \end{aligned} \quad (\text{B7})$$

In Eq. (B7), the $G_{LM, l' m'}^{lm}$ are the Gaunt coefficients which are defined by

$$G_{LM, l' m'}^{lm} = \int d\hat{r} Y_{lm}(\hat{r}) Y_{LM}^*(\hat{r}) Y_{l' m'}(\hat{r}). \quad (\text{B8})$$

Equations (B1) and (B7) are the expressions used to evaluate the current matrix elements.

*Work performed for the U.S. Energy Research and Development Administration under Contract No. W-7405-eng-82.

† Present address: Argonne National Laboratory, Argonne, Ill. 60439.

¹A. M. Clogston, V. Jaccarino, and Y. Yafet, Phys. Rev. **134**, A650 (1964).

²C. Stassis, G. R. Kline, and S. R. Sinha, Phys. Rev. Lett. **31**, 1498 (1973); Phys. Rev. B **11**, 2171 (1975).

³R. M. Moon, W. C. Koehler, and A. L. Trego, J. Appl. Phys. **37**, 1036 (1966).

⁴S. Asano and J. Yamashita, J. Phys. Soc. Jpn. **23**, 714 (1967).

⁵A. J. Freeman and R. E. Watson, Acta Crystallogr. **14**, 231 (1961).

⁶R. Huguenin, G. P. Pells, and D. N. Baldock, J. Phys. F **1**, 281 (1971).

⁷R. Kubo and Y. Obata, J. Phys. Soc. Jpn. **11**, 547 (1956).

⁸W. M. Lomer, Proc. Phys. Soc. Lond. **82**, 156 (1963); N. Mori, J. Phys. Soc. Jpn. **20**, 1383 (1965); Masaru Yasuri and Masao Shimizu, *ibid.* **31**, 378 (1971).

⁹J. E. Hebborn and N. H. March, Adv. Phys. **19**, 175 (1970).

¹⁰Y. Yafet, Phys. Rev. **106**, 679 (1957).

¹¹D. Pines, *Elementary Excitation in Solids* (Benjamin, New York, 1964).

¹²J. H. Van Vleck, *The Theory of Electric and Magnetic Susceptibilities* (Clarendon, Oxford, 1932), p. 227.

¹³C. Stassis, Phys. Rev. Lett. **24**, 1415 (1970).

¹⁴F. M. Mueller, J. W. Garland, M. H. Cohen, and K. H. Bennemann, Ann. Phys. (N.Y.) **67**, 19 (1971).

¹⁵D. D. Koelling, J. Phys. Chem. Solids **33**, 1335 (1972); B. N. Harmon and D. D. Koelling, J. Phys. C **7**, L210 (1974).

¹⁶B. N. Harmon and A. J. Freeman, Phys. Rev. B **10**, 1979 (1974).

¹⁷D. D. Koelling, A. J. Freeman, and F. M. Mueller, Phys. Rev. B **1**, 1318 (1970).

¹⁸L. F. Mattheiss, J. H. Wood, and A. C. Switendick, *Methods in Computational Physics* (Academic, New York, 1968), Vol. 8, p. 111.

¹⁹Both our wave functions and energies agree well with R. P. Gupta and S. K. Sinha [Phys. Rev. B **3**, 2401 (1971)]. The agreement with other band calculations is also good—see J. Rath and J. Callaway, Phys. Rev. B **8**, 5398 (1973), and references therein.

²⁰B. N. Harmon and H. Myron (unpublished).

²¹O. Jepsen and O. K. Anderson, Solid State Commun. **9**, 1763 (1971).

²²G. Lehman and M. Taut, Phys. Status Solidi B **54**, 469 (1972).

²³A. J. Freeman, B. N. Harmon, and T. J. Watson-Yang, Phys. Rev. Lett. **34**, 281 (1975).

²⁴Per-Anker Lindgård, Solid State Commun. **16**, 481 (1975).

²⁵J. Rath and A. J. Freeman, Phys. Rev. B **11**, 2109 (1975).